

Effects of Axial Ligands on the Formation of a Layered Structure in Mono- and Di-Cationic Charged Tetraphenylporphyrinatoantimony(V)/ Synthetic Clay Composites

Tsutomu Shiragami,* Keiko Nabeshima, Satoko Nakashima, Jin Matsumoto, Shinsuke Takagi,[1] Haruo Inoue,[1] and Masahide Yasuda

Department of Applied Chemistry, Faculty of Engineering, University of Miyazaki, Gakuen-Kibanadai, Miyazaki 889-2192

[1]CREST, JST (Japan Science and Technology Agency), 4-1-8 Honcho, Kawaguchi 332-0012

Received June 2, 2005; E-mail: t0g109u@cc.miyazaki-u.ac.jp

Novel metalloporphyrin–clay composites were prepared from a synthetic clay (Sumecton SA: SSA) and cationic tetraphenylporphyrinatoantimony(V) bromide (SbTPP, **1**–**4**) having various axial ligands. Both the crystal structure for SbTPP–SSA composites and the adsorption behaviors of SbTPP into SSA sheets are investigated regarding the relation to the structure of an axial ligand at SbTPP by measuring the X-ray diffraction (XRD), IR, UV–vis, and fluorescence spectroscopy. The XRD analysis revealed that powdered SbTPP–SSA composites could take a layered structure for **1**, and an amorphous structure for **2**, respectively. The IR spectrum of naked SSA showed a broad absorption band around 3000–3600 cm^{-1}, which can probably be assigned as some adsorbed water molecules onto SSA. The intensity of the broad absorption band became weaker with an increase of the loading level (%LL), which was defined as a ratio of the concentration of the cationic sites of **1**–**4** to the concentration of anionic sites of SSA. The band completely disappeared at 100%LL in both **2**–SSA and **4**–SSA composites with the amorphous structure, whereas the band remained even at 100%LL in both **1**–SSA and **3**–SSA composites with the layered structure. Information about an aggregation state of **1**–**4** into SSA was obtained by measuring both the UV–vis absorption spectra of **1**–**4** in an aqueous colloidal clay solution and the fluorescence spectra of SbTPP–SSA composites in the solid state by using a confocal laser scanning fluorescence microscope. Each spectral data indicated that the ammonium cationic part on an axial ligand of **1** only led to effective non-aggregated adsorption onto SSA sheets, while **2**–**4** were located with the aggregated state on SSA sheets. These results also support that an axial ligand structure can control not only the formation of the crystal structure, but also the adsorption behaviors with aggregation or non-aggregation onto SSA sheets.

The hybridization of some functional molecules into multilayered inorganic materials, such as clay minerals, is now attracting much attentions from the viewpoints of constructing inorganic/organic hybrid systems with new functionalities.[1–6] Clay minerals are known to provide two-dimensional spaces with highly ordered nano-structured environments for chemical reactions.[7–10] It is, therefore, expected that some organic compounds as guests adsorbed onto nano-clay sheets or intercalated nano-space interlayer can induce unique chemical behaviors by hybridization with clays as inorganic hosts. Recently, several studies on the photochemical properties of dye molecules onto a clay surface, or in the interlayer space, have elucidated that aggregation caused a disadvantage for a photoreaction owing to a decrease of the excited-state lifetime.[7–20] Therefore, the control of dye aggregation is very important to make a photoreaction effective in a clay system. Our research group has recently reported that unique hybrids in which porphyrin derivatives having +4 pyridinium cationic substitutes adsorb on the synthetic cation-exchangeable smectite clay (Sumecton SA: SSA) at high density without aggregation.[21–24] This effect was explained as being a size-matching effect i.e., the distance between a positive charged site in porphyrin molecules is matched with negatively charged sites on the clay sheet. The photochemical energy transfer in the size-matching effect in the porphyrin–clay system proceeded efficiently.[24]

On the other hand, porphyrin and metalloporphyrin dyes are of interest because of their photochemical activity as well as their biochemical and catalytic functionality.[25] We have previously reported that tetraphenylporphyrinatoantimony(V) complexes (SbTPP) derivatives could work not only as sensitizers,[26–29] but also as photocatalysts.[30–35] In most reports on the porphyrin–clay system, porphyrins having +4 charged substituents at the meso-position (e.g. alkyl pyridinium salt) were used as guest molecules for clay, as described above. SbTPP complexes are a "+1 charged cationic complex" where the positive charge can delocalize in a π-electron system of a porphyrin ring and have two axial ligands. They are a different type from the +4 cationic pyridinium-type porphyrin complexes. Therefore, we have recently reported on the adsorption and intercalation of a new type of cationic SbTPP into SSA.[36–38] In recent reports, we elucidated that the formation of the crystal structure of SbTPP–SSA composites strongly depended on the change of the axial ligand structure with SbTPP. This result gives new significant information as to how to control both the orientation of the cationic porphyrin adsorbed onto the clay surface and the structure of the porphyrin–clay

Published on the web December 9, 2005; DOI 10.1246/bcsj.78.2251

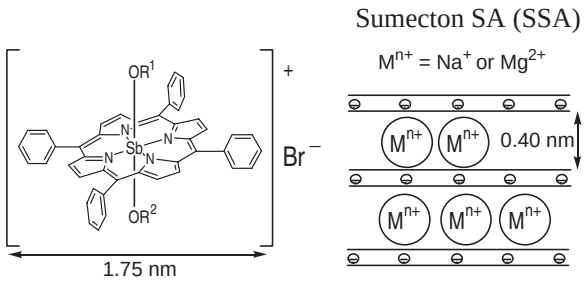

1a; R^1 = -$(CH_2)_3$-$\overset{+}{N}Me_3$ I^- R^2 = Me

1b; R^1 = -$(CH_2)_2$-O-$(CH_2)_2$-$\overset{+}{N}Me_3$ I^- R^2 = Me

2a; R^1 = -$(CH_2)_3$-NMe_2 R^2 = -Me

2b; R^1 = -$(CH_2)_2$-O-$(CH_2)_2$-NMe_2 R^2 = Me

3; R^1 = R^2 = H **4**; R^1 = R^2 = Me

Fig. 1. Structure of tetraphenylporphyrinatoantimony(V) complexes and SSA.

composite, revealing that the adsorption can be controlled by the position and structure of an interactive site located in the horizontal direction as well as the vertical direction for porphyrin plane. Since it was suggested that the effect of the axial ligand on the formation of the SbTPP–SSA composites structure could be attributed to a strong interaction between an axial ligand and the anionic clay sheets, the use of SbTPP having organo cations as an axial ligand, which are known to undergo interactions with the anionic clay sheets,[39] can be a clue to clarify the role of axial ligands in the SbTPP–SSA composites system.

In this paper, we report on the adsorption and intercalation behaviors of novel SbTPP **1** having an ammonium cationic part as an axial ligand (Fig. 1) into SSA in order to elucidate the relationships between the structure of the axial ligand and the formation of the layer structure of SbTPP–SSA composites or the SbTPP molecular orientation adsorbed into SSA sheets.

Experimental

Instruments. The UV–vis absorption spectra and fluorescence spectra of solutions were measured on a Hitachi U2001 spectrometer and on a Hitachi F4500 spectrometer, respectively. X-ray diffraction spectra (XRD) were measured on a RIGAKU RINT2500 spectrometer (Cu Kα, 40 kV/50 mA). IR spectra were measured on a JASCO Herscel FT/IR-300 spectrometer. ^{1}H NMR spectra were taken in $CDCl_3$ using tetramethylsilane as an internal standard on a Bruker AC 250P spectrometer at 250 MHz. Mass analysis was carried out by mass spectroscopy (SIMS method) on a Hitachi M-2000AM. Fluorescence spectra of powdered samples were measured on a confocal laser scanning fluorescence microscope (CLSM) (FV-300, Olympus) equipped with a spectrophotometer (STFL 250, Seki Technotron).

Materials. Sumecton SA (SSA) was received from Kunimine Industries Co., Ltd. and used without further purification. Water was deionized below 0.02 μS cm^{-1} of the conductivity with a MILLIPORE Elix 3 system equipped with a RO membrane module before use.

Synthesis of SbTPP Derivatives (1–4). The syntheses of **3** and **4** were performed according to a reported method.[30] The syntheses of **1** and **2** were carried out by the following procedures. The mono-methanolysis of dibromo(tetraphenylporphyrinato)antimony(V) bromide ($[SbTPP(Br)_2]^+Br^-$) was performed in MeOH–MeCN (1:1 v/v) to give $[SbTPP(Br)(OMe)]^+Br^-$. A MeCN–pyridine solution (5:1 v/v 50 mL) containing $[SbTPP(Br)(OMe)]^+Br^-$ (1.1 mmol) and *N*,*N*-dimethyl-3-amino-1-propanol (30 mmol) was heated for 2 h at 65 °C. The solvent was evaporated and the residue was solved in CH_2Cl_2. The CH_2Cl_2 solution was washed three times with 50 mL portions of H_2O. After evaporation, the crude product was chromatographed on silica gel (Fiji Silysia BW-300) using $CHCl_3$–MeOH (10:1 v/v) as an eluent to give **2a**. For methylation of the dimethylamino group, MeI (32 mmol) was added to a MeCN–pyridine solution (5:1 v/v 50 mL) of **2a** (1.1 mmol) and then heated for 2 h at 65 °C. The purification of **1a** was performed by a similar procedure for the case of **2a**. Complex **1b** was basically synthesized by a similar procedure with the synthesis of **1a**. A MeCN–pyridine solution (5:1 v/v 50 mL) containing $[SbTPP(Br)(OMe)]^+Br^-$ (1.1 mmol) and 2-(*N*,*N*-dimethylaminoethoxy)ethanol (30 mmol) was heated for 2 h at 65 °C, and then methylation of the dimethylamino group by MeI (32 mmol) to give **1b**.

3-Trimethylammoniopropoxo(methoxo)tetraphenylporphyrinatoantimony(V) bromide (**1a**): Yield 94% from **2a**; UV–vis (MeOH) λ_{max}/nm (log ε): 419 (5.48), 551 (4.15), and 591 (3.93); SIMS: m/z 881 ($M^+ - 2$); ^{1}H NMR ($CDCl_3$/ppm) δ −2.59 (2H, t, J = 6.0 Hz, –OCH_2–), −2.24 (3H, s, –OMe), −1.14 (2H, quint, J = 6.0 Hz, –CH_2–), 0.89 (2H, t, J = 6.0 Hz, –CH_2–$^+$N–), 2.18 (9H, s, –$^+NMe_3$), 7.83–8.00 (12H, m, Ph), 8.24 (4H, d, J = 6.6 Hz, Ph), 8.67 (4H, d, J = 6.6 Hz, Ph), 9.58 (8H, s, pyrrole).

3-(Dimethylamino)propoxo(methoxo)tetraphenylporphyrinatoantimony(V) bromide (**2a**): Yield 80%; UV–vis (MeOH) λ_{max}/nm (log ε): 419 (5.58), 551 (4.25), and 591 (4.09); SIMS: m/z 866 ($M^+ - 2$); ^{1}H NMR ($CDCl_3$/ppm) δ −2.65 (2H, t, J = 6.2 Hz, –OCH_2–), −2.29 (3H, s, –OMe), −1.58 (2H, quint, J = 6.2 Hz, –CH_2–), 0.20 (2H, t, J = 6.2 Hz, –CH_2–N–), 1.40 (6H, s, –NMe_2), 7.79–7.93 (12H, m, Ph), 8.23 (4H, d, J = 6.7 Hz, Ph), 8.34 (4H, d, J = 6.7 Hz, Ph), 9.48 (8H, s, pyrrole).

2-(2-Trimethylammonioethoxy)ethoxo(methoxo)tetraphenylporphyrinatoantimony(V) bromide (**1b**): Yield 40%; UV–vis (MeOH) λ_{max}/nm (log ε): 420 (5.68), 552 (4.29), and 591 (4.08); SIMS: m/z 911 (M^+); ^{1}H NMR ($CDCl_3$/ppm) δ −2.40 (2H, t, J = 4.7 Hz, Sb–OCH_2–), −2.14 (3H, s, –OMe), 0.35 (2H, t, J = 4.7 Hz, –CH_2–O–), 2.15 (2H, t, J = 5.0 Hz, –CH_2–$^+NMe_3$), 2.35 (9H, s, –$^+NMe_3$), 2.60 (2H, t, J = 5.0 Hz, –O–CH_2–), 7.95–8.09 (12H, m, Ph), 8.38–8.44 (8H, m, Ph), 9.69 (8H, s, pyrrole).

2-(2-Dimethylaminoethoxy)ethoxo(methoxo)tetraphenylporphyrinatoantimony(V) bromide (**2b**): Yield 36%; UV–vis (MeOH) λ_{max}/nm (log ε): 421 (5.68), 553 (4.29), and 593 (4.06); SIMS: m/z 896 (M^+); ^{1}H NMR ($CDCl_3$/ppm) δ −2.45 (2H, t, J = 4.7 Hz, Sb–OCH_2–), −2.20 (3H, s, –OMe), 0.18 (2H, t, J = 4.7 Hz, –CH_2–O–), 1.80 (2H, t, J = 5.0 Hz, –CH_2–NMe_2), 1.87 (6H, s, –NMe_2), 2.80 (2H, t, J = 5.0 Hz, –O–CH_2–), 7.93–8.04 (12H, m, Ph), 8.27–8.40 (8H, m, Ph), 9.57 (8H, s, pyrrole).

Results

Preparation of SbTPP–SSA Composites. SbTPP–SSA composites were prepared by mixing an aqueous SSA colloidal solution with the respective aqueous **1**–**4** solutions under sonication at room temperature. The SSA concentration was set to 50 mg dm^{-3} unless otherwise noted. The concentration of anionic sites in a colloidal solution of SSA was calculated to be 5.0×10^{-5} mol dm^{-3} from the cation exchange capacity (CEC) value of SSA.[22]

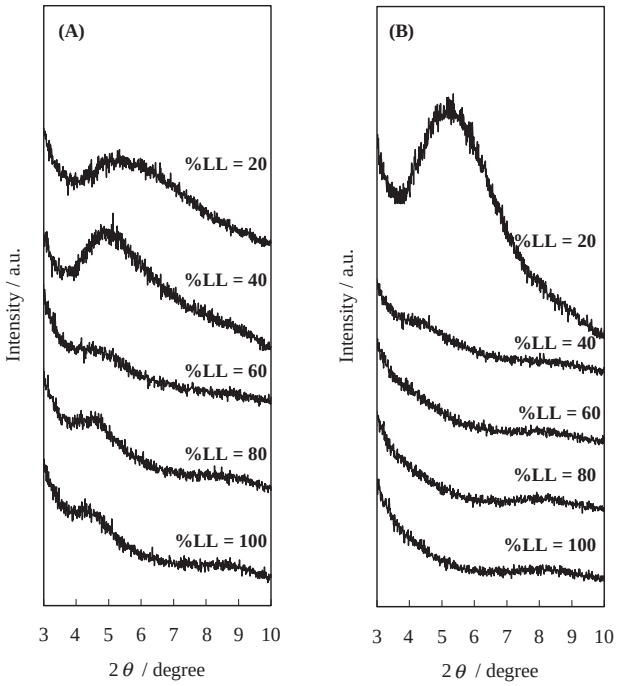

Fig. 2. The XRD profiles of (A) **1a**–SSA and (B) **2a**–SSA composites at various %LL.

The loading level (%LL) was defined as the ratio of the concentration of cationic sites of **1**–**4** to the concentration of the anionic sites of SSA. Various %LL were adjusted by the addition of a given amount of SSA (5.0×10^{-6}–5.0×10^{-5} mol dm^{-3}) to a solution of **1**–**4** (5.0×10^{-6} mol dm^{-3}). Measurements of the absorption spectra were performed for a colloidal solution of SbTPP–SSA complexes with various %LL at room temperature. The powdered complexes were collected by filtration of the mixture prepared above through a membrane filter (pore size = 1 μm) and dried at room temperature. They were then subjected to measurements of XRD, IR spectra (KBr method), and confocal laser scanning fluorescence microscope, respectively.

XRD Analysis of SbTPP–SSA Composite Powders. An XRD analysis was performed for the prepared samples by the filtration of colloidal SbTPP–SSA particles. The XRD profile of **1a**–SSA composites showed that the layer structure of SSA was kept at various %LL values irrespective of the addition of **1a** (Fig. 2A). Also, similar profiles were observed in the cases of **1b**–SSA and **3**–SSA composites. The interlayer distance strongly depended on the %LL of SbTPP. Figure 3 is a typical example for the case of the **1a**–SSA composite. The resulting interlayer distance became 1.03 nm for **1a**–SSA, 0.97 nm for **1b**–SSA, and 1.09 nm for **3**–SSA in more than 60%LL, respectively. On the other hand, the XRD profiles for the **2**–SSA and **4**–SSA composites showed no diffraction peaks, indicating the formation of the amorphous structure shown in Fig. 2B. Accordingly, these results obviously demonstrate that **2** and **4** can not intercalate into SSA with a layer structure, but only adsorb on the surface of SSA with an amorphous structure.

IR Spectra of SbTPP–SSA Composite Powders. As shown in Fig. 4, the IR spectrum of naked SSA gave a broad absorption band at around 3000–3600 cm^{-1}, which can be

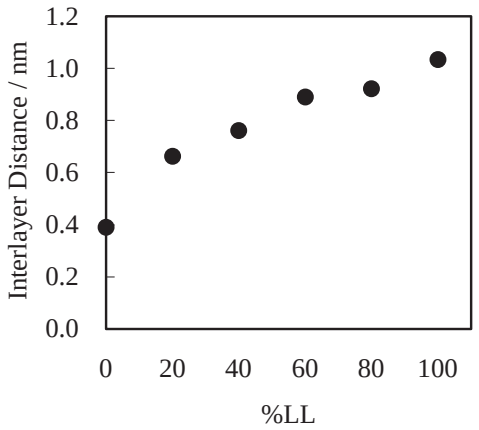

Fig. 3. Relationship between the %LL and the interlayer distance determined by XRD measurement of **1a**–SSA composite.

assigned to be O–H stretching vibration of adsorbed water molecules into SSA. The O–H band intensities of the **1a**–SSA composite decreased with an increase of %LL, but the O–H band remained even at 100%LL. A similar behavior was observed in the case of the **3**–SSA composite (Fig. 5). In the case of **2a**–SSA and **4**–SSA composites, on the other hand, the O–H band completely disappeared at 100%LL, as shown in Fig. 6. Figure 7 shows the dependence of %LL on a ratio of the peak area of the O–H band at each %LL to that of the naked SSA used as a standard. The **1a**–SSA and **3**–SSA composites having the layer structure can keep the adsorbed water molecules in the SSA layer.

Absorption Spectra of SbTPP–SSA Composites in an Aqueous Colloidal Solution. The λ_{max} of the Soret band of **2a** shifted to longer wavelength in ca.11–12 nm owing to adsorption onto the clay along with the broadening and splitting of the Soret band with an increase of %LL (Fig. 8). A similar spectral change was also observed in a colloidal SSA solution with **2b**. However, the absorption spectrum of **1a** showed a smaller red shift, though a broadening and splitting of the Soret band were not observed along with an increase of %LL, as shown in Fig. 8. This result indicates that the π–π interaction between the porphyrin rings with each other should be weaker in the case of **1a**. Since similar phenomena were also observed in the colloidal **1b**–SSA solution, the existence of a cationic part on an axial ligand can be a requisite for a non-broading and non-splitting of the Soret band in the SbTPP–SSA system. The absorption data of SbTPP–SSA composites are summarized in Table 1. All SbTPP (**1**–**4**) were adsorbed onto SSA quantitatively, because of no observation of the absorption peaks of **1**–**4** in their filtrates by the filtration of SbTPP–SSA powder. The quantitative adsorption onto SSA was also supported from the observation of free **1**–**4** in the colloidal SSA solution at 120%LL.

Fluorescence Spectra of SbTPP–SSA Composites in an Aqueous Colloidal Solution and Solid State. The fluorescence spectra were measured for a air-purged colloidal SbTPP–SSA solution with various %LL under excitation of the porphyrin chromophore at room temperature. The fluorescence quantum yield (Φ) was determined by using **3** (Φ =

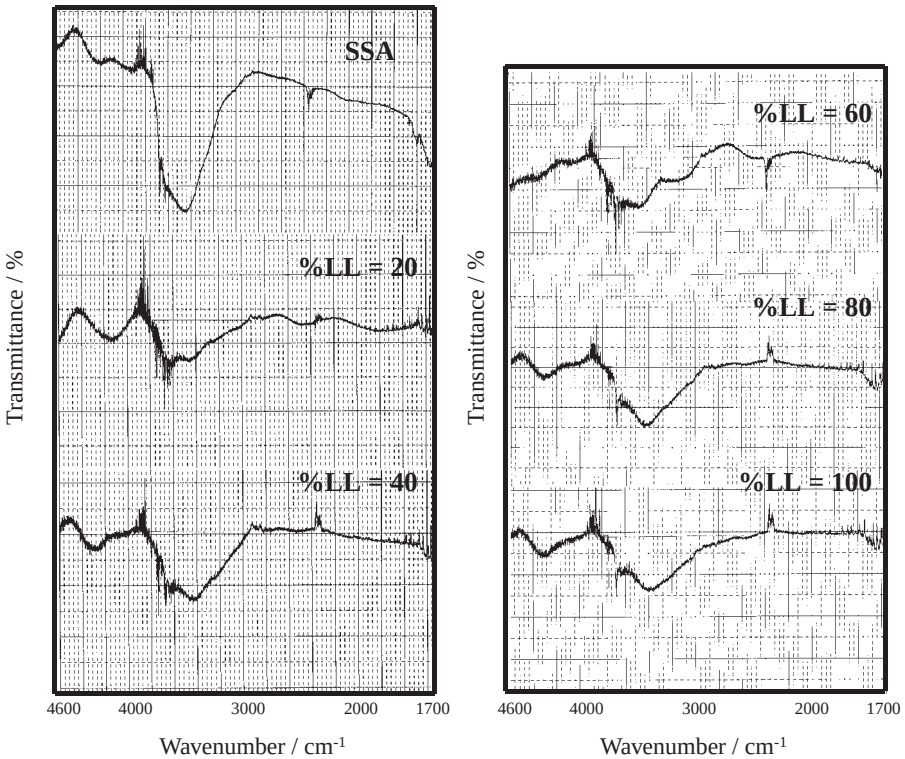

Fig. 4. IR spectra of SSA and **1a**–SSA composite at various %LL.

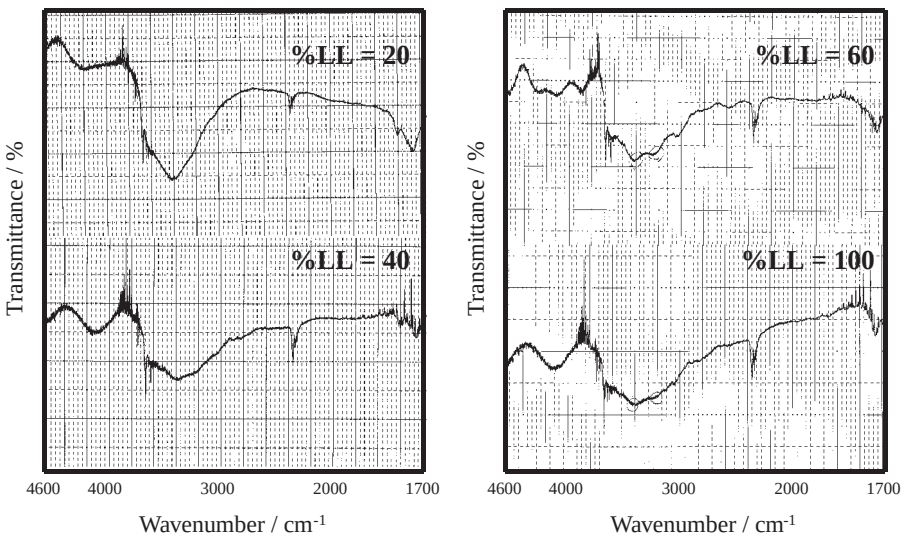

Fig. 5. IR spectra of **3**–SSA composite at various %LL.

0.0518 in MeCN) as an actinometer, according to the reported method.[28] Table 1 gives the fluorescence spectra and fluorescence quantum yield (Φ_f) of SbTPP–SSA composites. The λ_{max} values of the fluorescence spectra of **1**–SSA and **2**–SSA also show red shifts (ca. 7 nm) owing to adsorption onto the clay. In a previous report,[37] Φ_f of **3** adsorbed onto SSA (%LL = 80%) extremely decreased ($\Phi_f = 4.5 \times 10^{-3}$), compared with that of a MeOH solution of **3** ($\Phi_f = 45.6 \times 10^{-3}$), as shown in Table 1. On the other hand, the fluorescence quantum yield of **1a**–SSA was determined to be $\Phi_f = 29.3 \times 10^{-3}$. Figure 9 shows the fluorescence spectra of powdered SbTPP–SSA composites in the solid state by using CLSM. These spectra were observed at 40%LL of SbTPP–SSA composites and normalized at 620 nm. Interestingly, the shape of the fluorescence spectrum of **1a**–SSA was very close to that of **1a** in solution, whereas another SbTPP–SSA composite gave more broading fluorescence spectra, probably due to the aggregation of SbTPP into SSA.

Discussion

The results of an XRD analysis revealed that the structure of an axial ligand at SbTPP serves a crucial role to form a layered structure in the SbTPP–SSA composite. The **1**–SSA and **3**–SSA composites having a cationic part and an OH group as

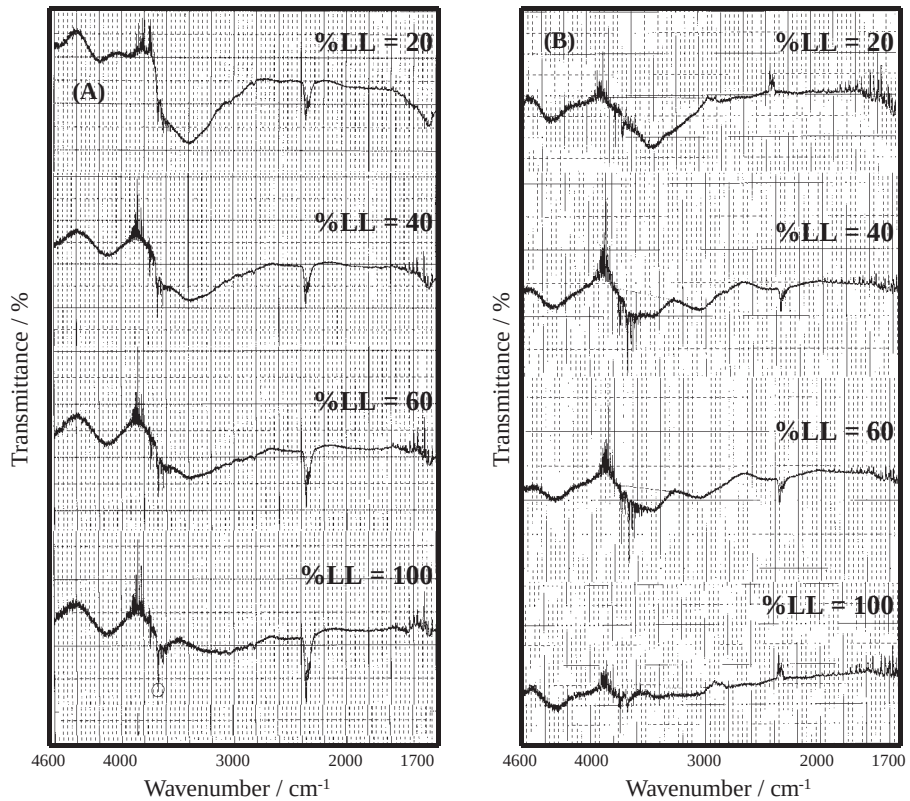

Fig. 6. IR spectra of (A) **2a**–SSA and (B) **4**–SSA composite at various %LL.

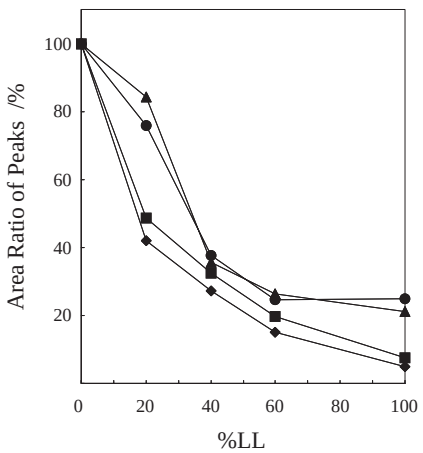

Fig. 7. Plots of %LL vs ratio of peak area of O–H band at %LL with that of naked SSA as standard; **1a** (–●–), **2a** (–■–), **3** (–▲–), and **4** (–◆–).

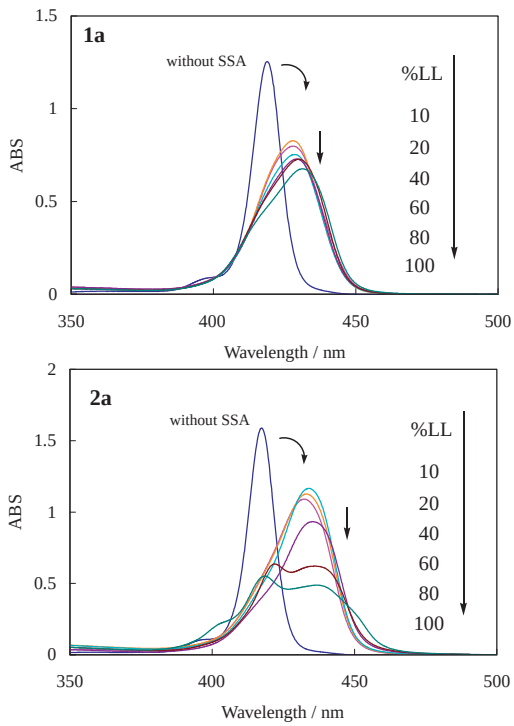

Fig. 8. Absorption spectra of **1a** and **2a** in aqueous colloidal SSA solution at various %LL.

an axial ligand can take a layered structure, respectively. An evaluation of the interlayer distance of **1**–SSA and **3**–SSA composites by XRD measurements can provide information on the orientation of **1** and **3** into SSA. The interlayer distance (1.03 nm) for the **1a**–SSA composite is closed to the thickness (0.94 nm) of **1a** for the axial ligand direction estimated by a PM3 calculation, as shown in Table 1. Also, the PM3 calculation of **1b**, having a longer chain as an axial ligand, gave a folded structure of an axial ligand chain as a most stable structure, resulting that the thickness of **1b** for an axial direction was estimated to be 0.86 nm. This value is almost the same as the interlayer distance (0.97 nm) of the **1b**–SSA composite. These results strongly suggest that **1** should be intercalated into the SSA interlayer space at high %LL, and that the orienta-

Table 1. Characteristic Data of SbTPP–SSA Composites

SbTPP	Soret band (λ_{max}/nm)			Fluorescence (λ_{max}/nm)		Φ_f /10^{-3}		Thickness /nm[a)]	Interlayer Distance/nm
%LL =	0	20	80	0	20	0[b)]	80		
1a	418	431	436	595	602	50.0	29.3	0.94	1.03
1b	419	431	421 442[c)]	595	602	—[d)]	—[d)]	0.86	0.97
2a	419	431	436	595	602	51.2	21.4	0.86	—
2b	418	431	419 443[c)]	595	602	—[d)]	—[d)]	0.86	—
3	417	430	430 445[c)]	594	600	45.6	4.5	0.42[e)]	1.09[f)]
4	417	431	430 445[c)]	594	600	48.8	6.4	0.73	—

a) Estimated by PM3 calculation for axial direction. b) Measured in methanol. c) Soret band was splitted. d) Not measured. e) Determined by X-ray crystallographic analysis (See Ref. 36). f) Two SbTPP molecules were intercalated into a interlayer of SSA (See Ref. 37).

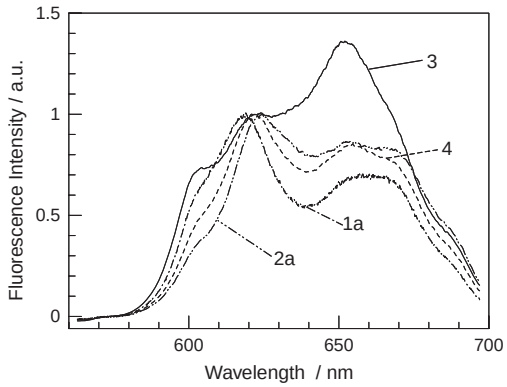

Fig. 9. Fluorescence spectra of the powdered SbTPP–SSA complexes by confocal laser scanning fluorescence microscope. These spectra were measured at 40%LL and normalized at 620 nm.

tion of the porphyrin plane should be almost parallel to the SSA sheets. If **1** is oriented vertically to the SSA sheets, the expanded interlayer distance should be about 1.75 nm.

The information on the orientation of **1** into the SSA interlayer space can also be estimated from the shape of the absorption and fluorescence spectra. Generally, it is well known that the absorption band of dye molecules adsorbed or intercalated into clay change to some broadening or splitting band, owing a strong π–π interaction stemming from a compact aggregation of dye molecules with each other.[40–43] In fact, larger broadening and splittings of the Soret band were observed in each colloidal SSA solution containing **2**–**4**. These spectral changes clearly indicate the aggregation of **2**–**4** onto the SSA surface, or in the interlayer space of SSA, as has been reported for another dye–clay system.[7–20] Fluorescence analysis on CLSM is very convenient for probing the orientation or aggregation of dye intercalated into clay under the powdered state, not the colloidal state. As shown in Fig. 9, the abnormal shape of the fluorescence spectra of **2**–SSA and **4**–SSA composites under the powdered state also shows the aggregation of **2**–**4** into SSA. However, the **1**–SSA system generated a quite different phenomenon concerning the behaviors of **1**.

We proposed that **1** should exist in a non-aggregated state in **1**–SSA composite, where their porphyrin rings could be located in an alternative orientation, such as head to tail. Figure 10 shows a plausible process for the formations of a layered structure of **1**–SSA and **3**–SSA through the coagulation process from the colloidal SbTPP–SSA composites. This speculation is supported by the following results: (1) The value of the expanded interlayer distance (1.03 nm) of SSA was not paradoxical with our proposition as for taking the parallel position for SSA sheets on the orientation of **1a** ring, as describe above, (2) the Soret band of **1a** showed neither a larger broadening nor splitting in a colloidal SSA solution, (3) the shape of the fluorescence spectrum of **1a** into SSA under a powdered state was very close with that of **1a** obtained in a solution, and (4) an extreme decrease of the fluorescence quantum yield in the **1a**–SSA composite was not observed, compared with much fluorescence quenching, such as in the **3**–SSA composite.

Since there is a relationship between the crystal structure of SbTPP–SSA composites and the disappearance of the O–H band with an increase of %LL, the presence of adsorbed water molecules can be operated for forming a layer structure of SbTPP–SSA composites. A cationic part and a hydroxy group on an axial ligand operates effectively to form a layer structure in **1**–SSA and **3**–SSA composites.

Conclusion

According to Fig. 10, nano-like SSA sheets are loosely aggregated in the colloidal state.[44] The coagulation from the loose aggregates can be accelerated by the adsorption of SbTPP. In fact, the rate of coagulation strongly depended on %LL of SbTPP, i.e. the coagulation of colloidal SbTPP–SSA composites at low %LL (10–40%) required several days in aqueous solution, whereas the colloidal SbTPP–SSA composites at high %LL (80–100%) coagulated required several hours in aqueous solution. These phenomena show that the coagulation process can be induced by a strong interaction between the axial ligand of SbTPP adsorbed on the first SSA sheet with the anionic site on the second SSA sheet. The interaction between an axial ligand part with second anionic SSA sheets should be regarded as a Coulombic attractive force for **1**–SSA composites or a hydrogen-bonding interaction for the **3**–SSA composite, respectively. Especially, the hydrogen-bonding networks formed by water molecules around the axial ligand should be a crucial factor for taking the more stable layer structure during the coagulation process for the **3**–SSA composite.

Since **1** has a cationic part on an axial ligand, the strong Coulombic attractive force with anionic SSA sheets can be at-

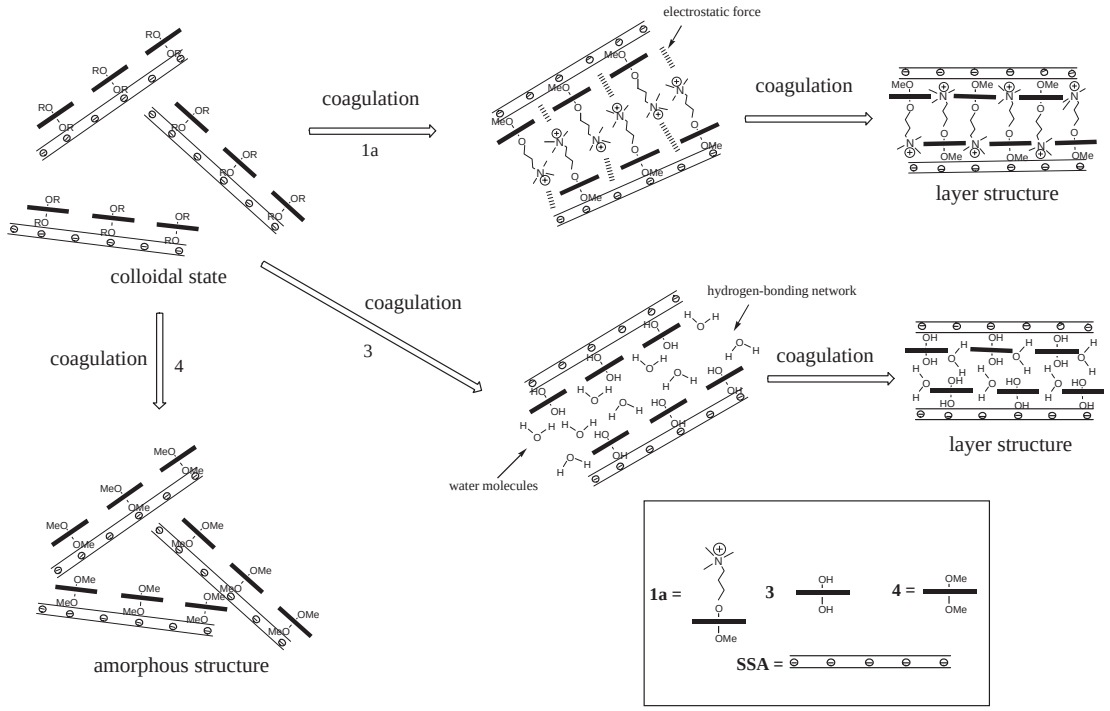

Fig. 10. Plausible process for the formation of layer structure through the coagulation of collidal SbTPP–SSA sheets and the supports of some water molecules around axial ligand.

tributed to suppressing the aggregation of **1** with each other on the SSA surface or in the SSA interlayer. Accordingly, it was clarified that the change of an axial ligand structure can affect not only the coagulation process for the formation of a crystal structure from colloidal SbTPP–SSA particles, but also an orientation and aggregation of SbTPP into SSA.

This research was supported by a Grand-in-Aid for Scientific Research (Nos. 16550127 and 15033258, Scientific Research in Priority Areas 417) from the Ministry of Education, Culture, Sports, Science and Technology. We are grateful to Mr. Kukizaki and Ms. Akazaki (Miyazaki Prefecture Industrial Technology Center) for XRD measurements.

References

1 J. K. Thomas, *Acc. Chem. Res.*, **21**, 275 (1988).
2 J. K. Thomas, *Chem. Rev.*, **93**, 301 (1993).
3 T. Kijima, *Thermochim. Acta*, **59**, 95 (1982).
4 K. Takagi and T. Shichi, "In Solid State and Surface Photochemistry," ed by V. Ramamurthy and K. S. Schanze, Marcel Dekker, New York (2000), Vol. 5, p. 31.
5 K. Takagi and T. Shichi, *J. Photochem. Photobiol., C*, **1**, 113 (2000).
6 M. Ogawa and K. Kuroda, *Chem. Rev.*, **95**, 300 (1995).
7 H. Usami, K. Takagi, and Y. Sawaki, *J. Chem. Soc., Faraday Trans. 2*, **88**, 77 (1992).
8 K. Takagi, T. Shichi, H. Usami, and Y. Sawaki, *J. Am. Chem. Soc.*, **115**, 4339 (1993).
9 S. S. Cady and T. J. Pinnavaia, *Inorg. Chem.*, **17**, 1501 (1978).
10 Z. Chernia and D. Gill, *Langmuir*, **6**, 1350 (1999).
11 K. A. Carrado and R. E. Winans, *Chem. Mater.*, **2**, 328 (1990).
12 H. Kaneyama, H. Suzuki, and A. Amano, *Chem. Lett.*, **1998**, 1117.
13 E. P. Giannelis, *Chem. Mater.*, **2**, 627 (1990).
14 I. Ukrainczyk, M. Chibwe, T. J. Pinnavaia, and S. A. Boyd, *J. Phys. Chem.*, **98**, 2668 (1994).
15 S. Bonnet, C. Forano, A. De Roy, and J. P. Besse, *Chem. Mater.*, **8**, 1965 (1996).
16 M. E. Perez-Bernal, R. Ruano-Casero, and T. J. Pinnavaia, *Catal. Lett.*, **11**, 55 (1991).
17 H. Tagaya, A. Ogata, T. Kuwahara, S. Ogata, M. Karasu, J. Kadokawa, and K. Chiba, *Microporous Mater.*, **7**, 151 (1996).
18 I. Park, K. Kuroda, and C. Kato, *Chem. Lett.*, **1989**, 2057.
19 L. Ukrainczyk, M. Chibwe, T. J. Pinnavaia, and S. A. Boyd, *Environ. Sci. Technol.*, **29**, 439 (1995).
20 Z. Tong, T. Shichi, K. Oshika, and K. Takagi, *Chem. Lett.*, **2002**, 876.
21 S. Takagi, T. Shimada, T. Yui, and H. Inoue, *Chem. Lett.*, **2001**, 128.
22 S. Takagi, T. Shimada, M. Eguchi, T. Yui, H. Yoshida, D. A. Tryk, and H. Inoue, *Langmuir*, **18**, 2265 (2002).
23 M. Eguchi, S. Takagi, H. Tachibana, and H. Inoue, *J. Phys. Chem. Solids*, **65**, 403 (2004).
24 S. Takagi, D. A. Tryk, and H. Inoue, *J. Phys. Chem. B*, **106**, 5455 (2002).
25 "The Porphyrin Hanbook," ed by K. M. Kadish, K. M. Smith, and R. Guliard, Academic Press, New York (1999).
26 Y. Andou, K. Shima, T. Shiragami, and M. Yasuda, *Chem. Lett.*, **2001**, 1198.
27 T. Shiragami, Y. Andou, Y. Hamasuna, F. Yamaguchi, K. Shima, and M. Yasuda, *Bull. Chem. Soc. Jpn.*, **75**, 1557 (2002).
28 Y. Andou, T. Shiragami, K. Shima, and M. Yasuda, *J. Photochem. Photobiol., A*, **147**, 191 (2002).
29 T. Shiragami, T. Tanaka, Y. Andou, S. Tsunami, J.

Matsumoto, H. Luo, Y. Araki, O. Ito, H. Inoue, and M. Yasuda, *J. Photochem. Photobiol., A*, **170**, 287 (2005).

30 T. Shiragami, K. Kubomura, D. Ishibashi, and H. Inoue, *J. Am. Chem. Soc.*, **118**, 6311 (1996).

31 T. Takagi, M. Suzuki, T. Shiragami, and H. Inoue, *J. Am. Chem. Soc.*, **119**, 8172 (1997).

32 S. Takagi, H. Morimoto, T. Shiragami, and H. Inoue, *Res. Chem. Intermed.*, **26**, 171 (2000).

33 T. Shiragami, Y. Shimizu, K. Hinoue, Y. Fueta, K. Nobuhara, I. Akazaki, and M. Yasuda, *J. Photochem. Photobiol., A*, **156**, 115 (2003).

34 H. Yokoi, T. Shiragami, J. Hirose, T. Kawauchi, K. Hinoue, Y. Fueda, K. Nobuhara, I. Akazaki, and M. Yasuda, *World J. Microbiol. Biotechnol.*, **18**, 559 (2004).

35 T. Shiragami, R. Makise, Y. Inokuchi, J. Matsumoto, H. Inoue, and M. Yasuda, *Chem. Lett.*, **33**, 736 (2004).

36 T. Shiragami, K. Nabeshima, J. Matsumoto, M. Yasuda, and H. Inoue, *Chem. Lett.*, **32**, 484 (2003).

37 T. Shiragami, K. Nabeshima, J. Matsumoto, M. Yasuda, and H. Inoue, *Res. Chem. Intermed.*, in press.

38 T. Shiragami, K. Nabeshima, M. Yasuda, and H. Inoue, *Chem. Lett.*, **32**, 148 (2003).

39 A. Okada and A. Usuki, *Mater. Sci. Eng., C*, **3**, 109 (1995).

40 M. Kasha, H. R. Rawls, and M. A. El-Bayoumi, *Pure Appl. Chem.*, **11**, 371 (1965).

41 R. H. Jin, S. Aoki, and K. Shima, *J. Chem. Soc., Faraday Trans.*, **93**, 3495 (1997).

42 K. Kano, T. Nakajima, and S. Hashimoto, *J. Phys. Chem.*, **91**, 6614 (1987).

43 H. L. Anderson, *Inorg. Chem.*, **33**, 972 (1994).

44 Y. Ogata, J. Kawamata, and A. Yamagishi, *Clays Clay Miner.*, **51**, 182 (2003).